

RESEARCH

Open Access



Corrosion of metal parts on satellites by iodine exposure in space

Daniel Zschätzsch^{1*} , Sebastian L. Benz¹, Kristof Holste¹, Max Vaupel², Franz G. Hey², Christine Kern³, Jürgen Janek³ and Peter J. Klar¹

*Correspondence:
Daniel.Zschaetzsch@physik.uni-giessen.de

¹ Institute of Experimental Physics I and Center for Materials Research (ZfM/LaMa), Justus Liebig University, Heinrich-Buff-Ring 16, 35392 Giessen, Germany

² Airbus Defence and Space GmbH, 88090 Friedrichshafen, Germany

³ Institute of Physical Chemistry and Center for Materials Research (ZfM/LaMa), Justus Liebig University, Heinrich-Buff-Ring 17, 35392 Giessen, Germany

Abstract

Iodine becomes increasingly popular as alternative propellant for electric propulsion (EP) systems offering several advantages over established xenon. However, iodine is also a reactive and corrosive element. Thus, a careful material selection for the EP system itself, but also for components employed on the satellite is required in the light of typical space mission durations of several years. Here, we carefully define an approach for mimicking long-term interaction of material specimens with iodine in a space environment. The space conditions cover typical iodine atmospheres (10^{-1} to 10^{-4} Pa), which occur in the vicinity of a satellite employing an iodine-fed EP system, and exposure times, which correspond to 10 years of mission duration. The approach is used to expose a wide range of metal specimens commonly used on spacecraft to iodine. Chemical modifications of the surfaces of the treated samples are analyzed by x-ray photoelectron spectroscopy (XPS). The elemental metals Fe, Ti, Al, and Nb chemically react with iodine, whereas the elemental metals Ni, Cr, Ta, W, and Mo are basically inert. The stainless-steel and aluminum metal alloys show the same behavior as the corresponding dominant elemental specimens, i.e., Fe and Al, respectively. Somewhat surprisingly, Cr as constituent in stainless steel reacts with iodine, in contrast to elemental Cr. Nevertheless, our studies reveal that long-term exposure to low-pressure iodine atmospheres is not critical for the macroscopic structural integrity of all tested specimens even over space mission durations of several years. The reaction with iodine is macroscopically a surface effect, which mainly affects the optical appearance.

Keywords: Electric propulsion, Iodine corrosion, Alternative propellants, Iodine atmosphere

Introduction

During the last decade electric propulsion (EP) systems, have developed from a niche technology into a mass product [1] enabling a large variety of scientific and commercial space missions. EP systems are used today on satellites ranging from nanosatellites [2] to large satellites [3] and are even considered as main propulsion systems for manned deep space missions [4]. The most widely used propellant in EP is the heavy noble gas xenon. However, xenon is a scarce resource and, therefore, expensive. Iodine is a possible alternative, since it is also a heavy atom, but much cheaper than xenon. In addition, no pressurized storage tanks are required for iodine, which further reduces the total

costs and enables an easier implementation into small satellites [5, 6]. Recently, Rafalskyi et al. [5] demonstrated the first satellite with an iodine-fed propulsion system in space. Satellites of mega constellations or cube sats are likely candidates to be equipped with iodine-fed EP systems. Therefore, it may be anticipated that the number of iodine-fed EP systems will significantly increase in the near future, in particular, if the potential danger of the corrosive nature of iodine can be controlled. Dedicated studies for assessing the effect of an iodine-rich space environment on typical materials used by space industry on satellites need to be conducted. An important aspect in this context is the definition of iodine-rich space conditions and their realization in terrestrial experiments since the reactivity of iodine may be strongly influenced by the presence of other substances. For example, water, which is typically not present in space, enhances the reactivity of iodine immensely [7].

General corrosive effects of iodine have been extensively investigated in the late twentieth century in the context of nuclear power plants [8–12]. Obviously, these studies did not mimic the particularities of space environments anticipated for iodine-fed satellites. In recent years, in the light of iodine as alternative EP propellant, first new studies were conducted to investigate the effects of iodine on materials used in the space industry [13–16]. These experiments have shown that iodine vapor can erode a wide range of materials on rather short time scales compared with typical spacecraft mission times of several years [17]. These experiments were mostly performed with dense iodine vapors or with a gas mixture, e.g., of iodine and an inert gas, with high iodine partial pressure. Such conditions correspond to those inside propellant feedlines and the thruster itself. However, these publications have not dealt with the effects of iodine on the outer surfaces of the satellite where the iodine densities or partial pressures are much lower. By expelling iodine, the amount of iodine in the spacecraft's surroundings is increased. The entire outer shell of the spacecraft will be in contact with the residual iodine. At such low iodine partial pressures, the exploratory focus is altered. The research question of interest is no longer whether a material is eroded by iodine, but rather how long may this material endure exposure to iodine without loss of structural integrity or the desired function.

In this work, we focus on the corrosive effect of iodine on a wide range of different metals. The exposure conditions used mimic the low-pressure environment in space experienced by satellites with iodine-fed EP systems over long mission durations. The first section explains and justifies how the space conditions are realized by terrestrial experiments. Furthermore, it gives details of the experimental setup and the samples studied. The following section presents the results of the analysis of the effect of iodine on the specimens studied. The last section summarizes the results and concludes the paper.

How to mimic space environment of satellites with iodine-fed EP systems?

Standard spacecraft components during satellite operation experience typically temperatures between -100 and $+100$ °C [18]. Higher temperatures generally promote chemical reactions; hence, we chose the upper limit of $+100$ °C in our experiments as it presents the worst-case scenario. Furthermore, when operating an iodine-fed EP system, different parts of the satellite are exposed to different iodine partial pressures. Typical

partial pressures inside the propellant feed system will be 2 to 6 kPa [5] and inside of the thruster about 1 to 2.5 Pa [19]. Outside the thruster, typical iodine partial pressure inside the plume will be about $1e-3$ Pa and will decrease with increasing distance from the satellite down to high vacuum conditions. A corresponding situation is illustrated in Fig. 1.

A prerequisite for a chemical reaction to occur is that the reaction partners come into contact. This implies microscopically that a collision between the reaction partners takes place. In our case, one of the reaction partners is a surface atom, which is bonded to other atoms of the solid, whilst the other one is a microscopic species of the atmosphere surrounding the satellite and colliding with its surface. Basically four microscopic species are generated by the electric thruster operating with iodine as propellant, for example, a radiofrequency ion thruster (RIT). These are the neutrals atomic I and molecular I_2 and the corresponding ionized species I^+ and I_2^+ . Molecular and atomic iodine ions, I^+ and I_2^+ , play a minor role in the context of surface erosion by the atmosphere as the plasma of an ion thruster is usually a low-temperature plasma. For example, global modelling of RITs operating with iodine as propellant reveals that only a few percent of the species inside the plasma vessel are ionized, the others are the neutral species [20, 21]. The same can be assumed for the species exiting the plasma vessel, either by diffusion or extraction by the grid system of the RIT. The main difference between ionic and neutral species is that the former move away from the thruster at high speed, typically several 10 km/s. Thus, the likelihood for ionic species to return to the satellite is rather low, in particular, as the ion beam is also neutralized by electrons. Therefore, ions will only cause erosion or sputtering if the ion beam extracted from the thruster directly hits the satellite surfaces. This will only occur unintentionally or by system failure. However, ion sputtering experiments on metallic and other samples demonstrate that, at typical ion energies of 1000 eV, the effect of ion etching by I^+ and Xe^+ , which possess comparable mass, is rather similar. Xenon ions are used for comparison as Xe is the still most

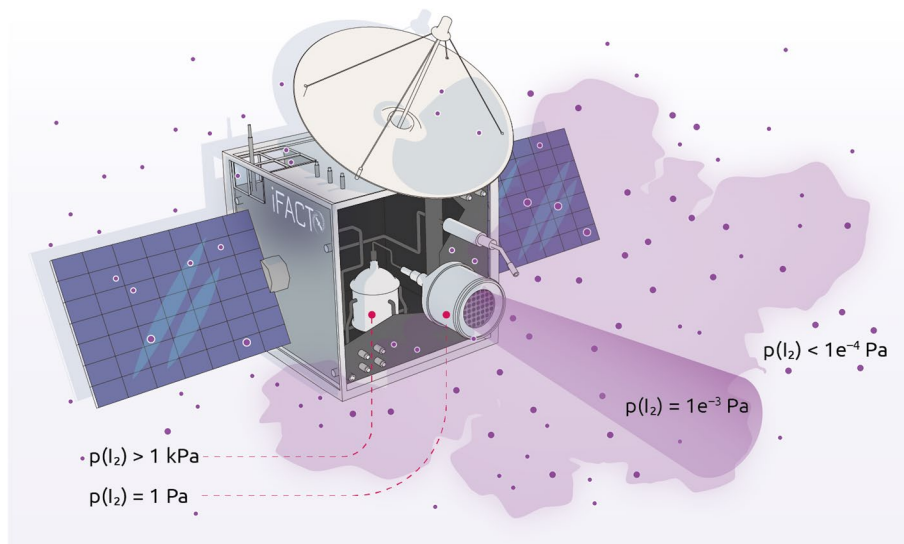


Fig. 1 A sketch of a satellite operating an iodine-fed electrical propulsion system. Typical iodine partial pressures are indicated

commonly used EP propellant. The similarity of the etching results implies that the etching process is not chemical, but dominantly physical by collisions [22]. Thus, the neutral species dominate the chemical behavior of the iodine atmosphere fed by the thruster and surrounding the satellite. There are the two types of neutral species which form the atmosphere around the satellite, molecular I_2 and atomic I. In the iodine plasma inside a RIT, both neutral species occur in roughly equal numbers whereas in our iodine gas treatment we have almost 100% I_2 . In the atmosphere surrounding the thruster, the atomic iodine will react to I_2 upon collision of atomic iodine, thus, will be lower than inside the thruster. However, it cannot be ruled out that in the steady state established in the atmosphere atomic iodine is still present. The fraction of iodine in the atmosphere, will depend on the operational conditions of the thruster and the mission scenario. If the thruster is not operated, the atmosphere will turn into an I_2 gas. We will show that this is not important in our considerations because the thermo-chemical considerations yield for the reaction of both species with the metals large and negative changes of the Gibbs free energy indicating that almost every collision triggers a chemical reaction and a back reaction is extremely unlikely. Therefore, a treatment of the metal surfaces with pure I_2 gas or a I_2 with a fraction of I should yield comparable results. Therefore, we only consider I_2 as reaction for the metals in what follows.

As pointed out above, a collision of an I_2 molecule with the surface is a prerequisite for the I_2 molecule to undergo a chemical reaction with the metal atoms of the surface. At low temperatures, the I_2 molecule may even be adsorbed. However, at the chosen temperature of 100 °C, the saturation vapor pressure is $p^* = 6$ kPa, which is much higher than the anticipated pressure in the satellite surroundings. Therefore, adsorption of iodine on the surface may be ruled out and the dominant contact mechanism of iodine molecules and the surface will be by collision. Not every collision leads to a chemical reaction. However, the likelihood of a chemical reaction to occur in a given time span is proportional to the collision frequency of the gas molecules with the surface per surface area, i.e., the particle current density and the exposure time Δt . The particle current density $J_{\text{Collision}}$ impinging on the surface can be described assuming that the ideal gas equation is valid [23],

$$J_{\text{Collision}} = \frac{p}{4k_B T} \cdot \sqrt{\frac{8k_B T}{\pi M}} \left[\text{collisions per s and m}^2 \right] \quad (1)$$

where T is the absolute temperature, p the partial pressure of the gas species, here iodine I_2 , k_B the Stefan-Boltzmann constant, and M is the molecular mass of the gas species (254 u = 4.22e-25 kg in case of I_2).

The terrestrial experiments mimicking the effect of iodine on a solid will be performed with the solid located inside a vessel of volume V with a gas mixture of iodine and the noble gas argon (see Fig. 2). Considering that no chemical reaction takes place between chemically inert Ar and I_2 in the gas mixture, both species are individually describable by the ideal gas equation $p_i V = N_i k_B T$ ($i = 1, 2$), where p_i and N_i denote the partial pressure and the number of particles, respectively, of species i inside V . Total pressure is the sum of the partial pressures $p_{\text{tot}} = p_1 + p_2$. This relation holds for gas mixtures of iodine and argon, despite the strong reactivity of iodine, if we assume an ideal gas solution.

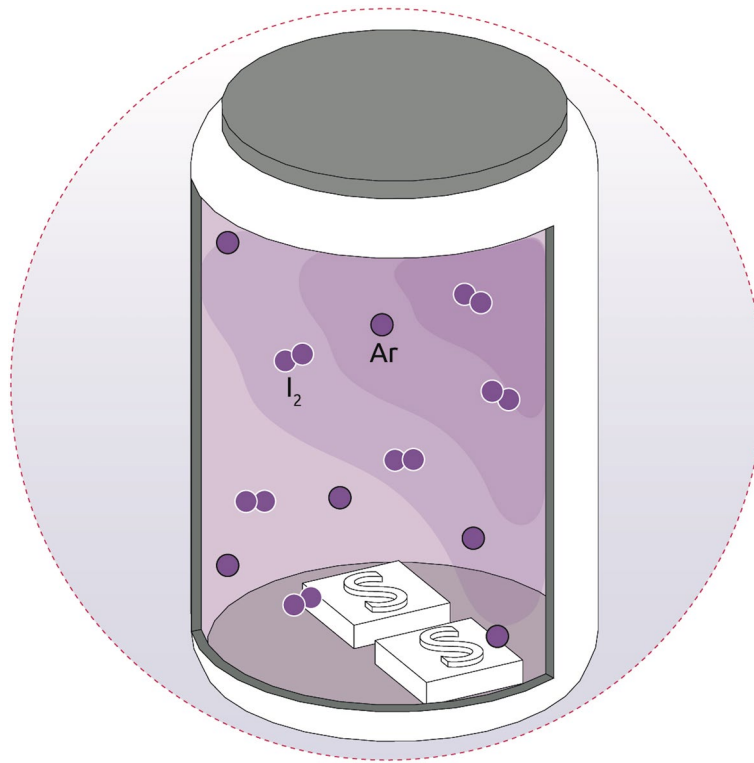


Fig. 2 Laboratory experiments for realizing different space scenarios representing the conditions in the surroundings of a satellite with an iodine-fed EP system. The samples are treated at 100 °C in a sealed glass vessel containing a defined amount of iodine and argon. The vessel V was loaded inside a glove box with a dry argon atmosphere at room temperature with the desired amount m of solid iodine and the cleaned samples, afterwards it is sealed. Heating the sample up to 100 °C allows one to fully or partially evaporate the iodine yielding partial pressures of iodine $p \leq p^*$

At 100 °C (373 K), iodine confined in a vessel of finite volume V will have a saturation vapor pressure of about $p^* = 6 \text{ kPa}$ as iodine partial pressure, as long as the inequality

$$m/V \geq (M \cdot p^*) / (N_A \cdot k_B \cdot T) \quad (2)$$

holds for the mass m of solid iodine stored inside the finite volume V . Partial pressures of iodine gas inside the reaction vessel, which are lower than its saturation vapor pressure p^* , can be obtained, if the mass m is smaller than that yielding equality in Eq. (2). In these cases, all the iodine in the vessel is in the gaseous state and its partial pressure is given by

$$p = \frac{m \cdot T \cdot N \cdot k_B}{V \cdot M} \quad (3)$$

Here, the number of surface atoms of the solid reacting with the impinging iodine molecules at a given temperature T is to a first approximation proportional to $J_{\text{Collision}} \propto p$ (where p denotes the partial pressure of iodine) and the exposure time Δt . This implies that pairs $(p, \Delta t)$ yielding the same value for the product $p \cdot \Delta t$ will have a similar effect on the surface. The approximation is particularly suitable to mimic the effects

in low-pressure iodine environments over long periods of time, as experienced in space missions, by choosing higher pressures and shorter exposure times in the terrestrial experiments.

At 100°C (373 K), iodine reaches its saturation vapor pressure p^* of about 6 kPa only if a sufficient amount of solid iodine is located in the finite volume V . The corresponding $J_{Collision}$ multiplied with an exposure time $\Delta t = 3$ h leads to a value of about $6e29$ collisions per m^2 with a solid surface in contact with the gas. The same total number of collisions per m^2 is obtained for another $(p, \Delta t)$ -pair, namely $p = 0.1$ Pa at 100°C and $\Delta t = 10$ years, which is typical for what satellite components outside, but in the vicinity of the iodine-fed EP system, may experience.

In this fashion, we designed a set of exposure experiments intended to mimic the effect of iodine on outside satellite components for environmental iodine partial pressures p of $1e-2$, $1e-3$, and $1e-4$ Pa and a mission duration of 10 years. This is achieved by reducing the partial pressure of iodine inside the reaction vessel by increasing its volume V or by reducing the amount of iodine m inside the vessel according to Eq. (3) or by reducing the exposure time Δt .

Some additional aspects need to be considered to justify our approach. A reduction of the iodine partial pressure reduces the number of collisions very effectively, but a reduced partial pressure (below the saturation vapor pressure) has also an influence on the chemical reactions from a thermodynamic point of view going beyond the ideal gas approximation. A chemical reaction will be exergonic (spontaneous) only, if the change of Gibbs free energy is negative, i.e., free energy is released over the course of the reaction. The change of Gibbs free energy for a specific chemical reaction ($\Delta_r G^T$) at temperature T is given by

$$\Delta_r G^T = \sum v_i \cdot \Delta_f G_i^T \quad (4)$$

Large negative values of $\Delta_r G^T$ indicate a self-driven (more exergonic) reaction. At constant pressure and constant temperature, the Gibbs free energy for the reaction depends only on Gibbs free energy ($\Delta_f G^T$) and molar coefficients (v_i) of the reactants and products involved in the chemical reaction. The molar coefficient for the reaction educts is of a negative sign whereas that the reaction products is positive by convention. The standard enthalpy of formation $\Delta_f H^T$ and standard entropy S^T for all kinds of substances, e.g., $I_{2(g)}$, FeI_2 , etc. can be found in the literature for the temperature T of interest [24]. This data is used to calculate the available energy ($\Delta_f G^T = \Delta_f H^T - T^* S^T$). Above, we have assumed that the outcome of the exposure experiment is the same if the product of $p \cdot \Delta t$ is equal for the two scenarios and the temperature kept constant. This implies that the change of Gibbs free energy $\Delta_r G$ according to Eq. (4) for the surface reaction involving iodine is independent of iodine partial pressure. Nevertheless, the validity and the boundaries of this assumption needs to be verified. The molar coefficients v_i do not depend on iodine partial pressure. However, the Gibbs free energy of iodine exhibits a dependence on partial pressure for iodine in its gaseous form:

$$\Delta_f G^{T*}(I_2) = \Delta_f G^T(I_2) + RT \cdot \ln \left(\frac{p(I_2)}{p^c} \right) \quad (5)$$

Table 1 The change of Gibbs free energy for gaseous iodine at different iodine partial pressures for $p^c = 10^5$ Pa and $T = 100^\circ\text{C}$. Values are given in kJ/mol

$p(\text{I}_2)$ [Pa]	$RT \cdot \ln \left(\frac{p(\text{I}_2)}{p^c} \right)$	$\Delta_f G^{T*}(\text{I}_2, p(\text{I}_2))$
1e-04	−64.27	−104.20
1e-03	−57.12	−97.06
1e-02	−49.98	−89.92
1e-01	−42.84	−82.78
15	−27.30	−67.24
200	−19.27	−59.21
2000	−12.13	−52.07
6000	−8.72	−48.66

Table 2 Calculated values of Gibbs free energy ($\Delta_r G^T$) at 100°C of possible iodine reaction scenarios following Eq. 6. Literature values for $\Delta_f G^T$ are taken from [24] and are given in kJ/mol

Product $p(\text{I}_2)$ [Pa]	Al_3	CrI_2	CrI_3	CuI	FeI_2	MgI_2	MoI_2	NiI_2	TlI_4	ZnI_2
1e-04	−202.6	−106.9	−113.3	−41.7	−57.5	−304.0	−49.7	−25.2	−257.5	−147.4
1e-03	−213.3	−112.1	−124.0	−45.3	−64.6	−311.1	−56.8	−32.4	−271.8	−154.5
1e-02	−224.0	−119.3	−134.8	−48.8	−71.7	−318.2	−64.0	−39.5	−286.1	−161.7
1e-01	−234.7	−126.4	−145.5	−52.4	−78.9	−325.4	−71.1	−46.6	−300.4	−168.8
15	−258.0	−142.0	−168.8	−60.2	−94.4	−340.9	−86.6	−62.2	−331.4	−184.4
200	−270.1	−150.0	−180.8	−64.2	−102.5	−348.9	−94.7	−70.2	−347.5	−192.4
2000	−280.8	−157.1	−191.5	−67.8	−109.6	−356.1	−101.8	−77.4	−361.8	−199.5
6000	−285.9	−160.5	−196.6	−69.5	−113.0	−359.5	−105.2	−80.8	−368.6	−202.9
$\Delta_r G^T(\text{Product})$	−371.6	−221.9	−280.5	−108.4	−174.0	−422.3	−166.6	−142.9	−479.3	−269.1

where R is the ideal gas constant, $p(\text{I}_2)$ the partial pressure of iodine inside the reaction vessel, and p^c is the reference pressure of the standard conditions (10^5 Pa). The effect of the additional term is given in Table 1 for different partial pressures of iodine.

In this work, we consider the reaction of gaseous iodine with a solid metal A. As example, the chemical reaction between Fe and I_2 can be written as $\text{Fe}_{(s)} + \text{I}_{2(g)} \rightarrow \text{FeI}_{2(s)}$. The molar coefficients are -1 , -1 , and 1 , respectively from left to right. Hence, Eq. 4 is rewritten as:

$$\Delta_r G^T(\text{FeI}_2) = \Delta_f G^T(\text{FeI}_2) - \Delta_f G^T(\text{Fe}) - \Delta_f G^{T*}(\text{I}_2, p(\text{I}_2)) \quad (6)$$

The literature values for $\Delta_f G^T$ of the substances at $T = 100^\circ\text{C}$ are -174.0 kJ/mol and -12.3 kJ/mol for FeI_2 and Fe, respectively. The tabulated values for $\Delta_f G^{T*}(\text{I}_2, p(\text{I}_2))$ at the different iodine partial pressures are given in Table 1. We find that $\Delta_r G^T$ is always negative, thus, the reaction is exergonic. Furthermore, $\Delta_r G^T(\text{FeI}_2)$ is only about 16% lower at a partial iodine pressure of 15 Pa compared to the value at 6 kPa partial iodine pressure, which is the saturation pressure of the test conditions. A change of this magnitude is to a first approximation negligible in terms of chemical reactivity, since the reaction remains strongly exergonic in all conditions. Nevertheless, reducing the iodine partial pressure by multiple orders of magnitude, as present in space, leads to a significant reduction of $\Delta_r G^T$ and, therefore, a less, but

still, exergonic reaction. Conclusions similar to those drawn from the FeI_2 reaction hold true for all expected products as shown in Table 2. Conducting the same calculation for atomic iodine using the corresponding thermo-chemical data [25] yields the same trends for $\Delta_r G^\text{T}$ with 1.5 times higher values. As pointed out above, this means in both cases that the back reaction is suppressed. Whether the reaction of the metal with I or I_2 is more likely cannot be decided based on the corresponding $\Delta_r G^\text{T}$ values.

Another aspect, which we ignore in the design of the experiment, is that during exposure the sample surface is converted into reaction products, i.e., less metal atoms per m^2 are available as reaction partners as the exposure progresses. Our scaling law, which assumes that scenarios with the same $(p \cdot \Delta t)$ yield similar effects, may no longer be valid, if the chemical reaction region extends deep into the interior of sample as the transport of iodine within the solid will very likely depend on Δt despite the same T . Thus, the exposure experiments conducted are the more representative for the long-term exposure to iodine under space conditions, the thinner the surface region where the chemical reaction takes place. As will be seen later, this condition is fulfilled for all samples analyzed in this work. The maximum thickness found after treatment with the harshest conditions (scenario 4) is about $20 \mu\text{m}$.

The assumption that the saturation pressure of iodine is independent of the presence of Ar in the gas mixture inside the reaction vessel is an approximation only. The presence of an argon atmosphere alters the phase diagram of iodine only slightly. The correlation between saturation vapor pressure p^* and the total pressure p_{tot} in a gas mixture is expressed by the inequality

$$\frac{\delta \ln(p^*)}{\delta p_{\text{tot}}} \geq 0. \quad (7)$$

Equation 7 shows that by increasing p_{tot} the vapor pressure may increase. Hence, the iodine vapor is possibly somewhat denser in the presence of the argon atmosphere in the exposure experiments than it would be in the presence of vacuum. This implies that the damage in space due to corrosion will be slightly overestimated.

In summary, the reaction of iodine with a sample depends mainly on the collision frequency and the chemical potentials. In case of metals reacting with iodine, the impact of the partial pressure p and the type of species I_2 or I on the chemical potentials and thus on the likelihood of the reaction taking place is rather small as the reactions are very exergonic. Thus, samples treated in scenarios A and B according to the relation $(p_A \cdot \Delta t_A) = (p_B \cdot \Delta t_B)$ where p_i ($i = A, B$) is the iodine pressure and Δt_i the exposure time in each case will not show quite the same degree of corrosion despite the same number of collisions of iodine molecules with the surface during exposure. However, the discussion shows that the degree of erosion of the sample treated in scenario A must be higher than in scenario B, if $p_A > p_B$. Therefore, our approach of mimicking the damage at low pressure p_B and long duration Δt_B (i.e., during a space mission) by exposure experiments at higher p_A and shorter duration Δt_A (i.e., in the laboratory) yields an upper limit for the degree of damage caused during the space mission, as the assessment of the damage is based on the sample treated in scenario A. In this sense, simulating long-term and low-pressure cases in space by short-term

and high-pressure cases in laboratory is justified. However, it needs to be kept in mind that the results give an upper boundary for the severity of the corrosion effects, i.e., this intrinsically gives a safety margin.

Experimental setup

We studied a variety of elemental metals as well as metal alloys. The composition of the metal alloys are listed in Table 3.

Iodine exposure experiments were conducted in four different scenarios corresponding to four different ($p \cdot \Delta t$) values to mimic space flights of 10 years in environments with iodine partial pressures of 1e-4, 1e-3, 1e-2, and 1e-1 Pa. A comparison of the conditions in space and those used to simulate them in the laboratory are given in Table 4. It should be noted that the realization in the laboratory employs a gas mixture of iodine and argon. The partial pressure p of I_2 in the reaction vessel is listed in the table, that of Ar was constant at about 10^5 Pa in all scenarios. As discussed in the previous section, the presence of Ar does not affect the outcome of the experiment.

The workflow of the exposure experiments including the subsequent XPS characterization is shown in Fig. 3. The metallic samples with sizes of 11 mm \times 11 mm \times 2 mm were ultrasonically cleaned in isopropanol, prior to inserting them into the glass

Table 3 List of samples studied. Top list: stainless steel, aluminum, and titanium alloys of various compositions (data from ISO standards). Only the mass fractions of the dopant constituents are listed, not of the hosts, i.e., iron (Fe), aluminum (Al), and titanium (Ti). Bottom list: elemental metal samples and their purity (given by the supplier)

Alloy name	Maximal mass fraction of alloy element
Stainless steel	
1.4404	17.5% Cr, 12.5% Ni, 2.5% Mo
1.4544	19.0% Cr, 12.0% Ni, 0.7% Ti
1.4546	19.0% Cr, 11.5% Ni, 1% Nb
1.4571	18.5% Cr, 13.5% Ni, 2.5% Mo, 0.7% Ti
1.4301	19.5% Cr, 10.5% Ni
1.4401	18.5% Cr, 13.0% Ni, 2.5% Mo
Aluminum alloys	
EN AW-5754	0.2% Zn, 3.6% Mg, 0.1% Cu, 1.3% Si
EN AW-6082	0.2% Zn, 1.2% Mg, 0.1% Cu, 1.3% Si
EN AW-7075	6.1% Zn, 2.9% Mg, 2.0% Cu, 0.4% Si
Titanium	
Ti 2 (3.7035)	0.3% Fe, 0.08% C, 0.03% N, 0.25% O
Element Name	Bulk Purity
Elemental Samples	
Al	> 97.5%
Cr	99.99%
Fe	99.5%
Mo	> 98% ^a
Nb	99.9%
Ni	99.99 + %
Ta	99.9%
W	> 98% ^a

^a based on our analysis of the XPS survey spectra

Table 4 Conditions in space and those used to simulate them in the laboratory experiments. In the laboratory experiments a gas mixture of iodine and argon is employed. The partial pressure p of I_2 in the reaction vessel is listed, that of Ar was about 10^5 Pa in all scenarios. In scenario 4, the ratio m/V fulfills the inequality in Eq. (2), i.e., $p = p^*$ for iodine

	Space conditions @ 100 °C		Lab conditions @ 100 °C		Realization	
	p [Pa]	Δt [y]	p [Pa]	Δt [min]	m [g]	V [mL]
Scenario 1	1e-4	10	15	36	1.3e-3	1062
Scenario 2	1e-3	10	200	30	1.74e-2	1062
Scenario 3	1e-2	10	2000	30	0.174	1062
Scenario 4	1e-1	10	6000	180	1	135

reaction vessel. The desired amount of solid iodine was added. The entire loading process took place at ambient temperature inside a glove box with a dry Ar atmosphere to exclude contact of the samples and the high-purity iodine with air and humidity as, in particular, iodine is hygroscopic [26]. The iodine used was provided by Th. Geyer Company was of 99.999% purity. The argon atmosphere inside the glove box was not directly monitored; however, a flow of pure argon and a bowl of dry beads reduced the O_2 and H_2O content to a minimum. After loading, the glass reaction vessel inside the glove box was sealed with a glass lid and a rubber seal. Thus, it contains the Ar atmosphere, the samples, and the solid iodine. The sealed reaction vessels were removed from the glove box and placed inside a preheated oven at 100 °C where the iodine evaporates (i.e., only partially in case of scenario 4) yielding the desired iodine partial pressures given in Table 4. After the desired exposure time, the sealed vessels were taken out of the oven for cooling down. Afterwards, the reaction vessel was transferred back into the glove box. There, the samples were removed from the vessel and stored in the Ar atmosphere to evaporate residual I_2 . All characterization experiments took place in the absence of air, either inside the glove box or in vacuum. The gravimetric analysis was performed on the balance inside the glove box. In case of the

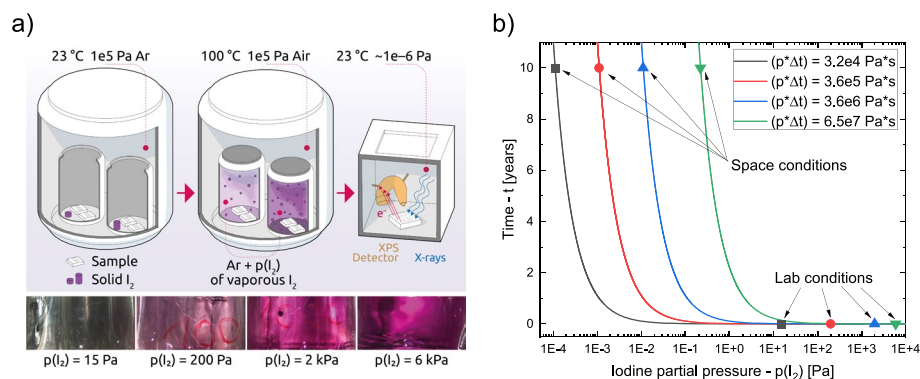


Fig. 3 a Top: Workflow of the sample exposure to iodine and subsequent characterization by XPS. Bottom: Photographs of iodine vapor of different density inside the reaction vessels in scenario 1 (left) to 4 (right). The partial pressures of iodine realized are given below the photographs. b Plots of exposure time Δt versus logarithm of the iodine partial pressure p for constant $(p \cdot \Delta t)$ for the four test scenarios. Space conditions and laboratory conditions are indicated on the curves

XPS experiments, a transfer module was used to insert the sample into the XPS without contact to air and humidity.

The color photographs of the interior of the glass reaction vessel heated to 100°C reveal how the optical transparency of the iodine vapor decreases and the purple color intensifies with increasing iodine partial pressure, when going from scenario 1 to 4. The right graph shows the plots of constant ($p \cdot \Delta t$) which connect the laboratory conditions of scenario 1 to 4 with the corresponding space conditions.

The XPS measurements were conducted with a PHI Versaprobe II spectrometer at room temperature. A monochromatic Al-K $_{\alpha}$ (1486.6 eV) x-ray anode provides the excitation at an angle of 45° to the surface normal in an ultra-high vacuum environment (pressure of about 10⁻⁶ Pa). Narrow-range spectra of the core level signals were recorded with a pass energy of 23.5 eV at an energy resolution of 0.2 eV, while the survey spectra were recorded with a pass energy of 93.9 eV and an energy resolution of 0.8 eV. From each sample, narrow-range spectra were measured of the core levels O 1s, C 1s, and I 3d. Additionally, spectra of the core level regions of the constituting elements, e.g., Al 2p, Cr 2p, Fe 2p, Mo 3d, Nb 3d, Ni 2p, Ta 4f, Ti 2p, and W 4f depending on the sample composition, were recorded. Set of measurements were recorded at the surface of the sample, after 120 s, and after 240 s of Ar⁺-etching with 1 kV acceleration voltage. The etching depth is in the order of nm (< 10 nm). Charge neutralization was achieved during etching and data collection by compensating the positive charges from the Ar⁺-gun by negative charges from an electron-gun. The collected XPS data was analyzed using the CasaXPSTM software. The spectra $S_{\text{ref}}(E)$ and $S_{\text{treated}}(E)$ were post-referenced to the peak position of adventitious carbon (284.8 eV). All spectra were background corrected with a Shirley-background $B(E)$ and fitted with multiple Voigt-functions of a 60% or 30% Lorentz quota to analyze the energy position and area of the core level signals. The metallic signals were fitted with a Lorentzian asymmetric line shape according to the given references.

The spectra of the reference and iodine treated sample, $S_{\text{ref}}(E)$ and $S_{\text{treated}}(E)$, are combined to a difference spectrum $\Delta S(E)$ which highlights the changes caused by the iodine treatment. The difference spectrum is calculated as follows

$$\Delta S = \frac{2 \cdot [(S_{\text{treated}} - B_{\text{treated}}) - (S_{\text{ref}} - B_{\text{ref}})]}{S_{\text{treated}} + S_{\text{ref}}} \quad (8)$$

The calculation of ΔS does not include any normalization, because it was not possible to generate comparable result for all materials. Consequently, the calculation procedure has the disadvantage that it does not compensate a reduced detection signal by a damping iodine layer. Thus, we generally expect a slightly negative area, if an iodine layer without chemical reaction in form of I₂ covers the surface.

The portions of solid iodine inserted into the reaction vessels and the metallic samples prior and after iodine exposure were weighed inside the glove box using a Mettler Toledo AB analytical balance with an accuracy of 0.1 mg.

The time-of-flight secondary ion mass spectrometry (ToF-SIMS) measurements for determination of iodine diffusion were performed with a M6 Hybrid SIMS instrument (IONTOF GmbH) equipped with a 30 keV Bi cluster primary ion gun for analysis. All ToF-SIMS measurements were conducted in negative ion mode using Bi₃⁺ ions as

primary ion species since iodine forms predominately negative ions in SIMS analyses. The depth profiling was realized by using an additional dual-source column, which was operated with 2 keV Cs^+ in a non-interlaced mode (sputter current about 100 nA). Measurement cycle of ToF-SIMS depth profiling with alternating analysis and sputtering steps results in diffusion profiles, mass spectra, and 3D mass image maps. Charge compensation was realized by flooding the surface with low-energy electrons for 3 s between each analysis and sputtering step. The following signals were used for mass calibration: F^- , C_2^- , S^- , Cl^- , C_3^- , I_2^- . For analysis, the primary ion gun was operated in the spectrometry mode (bunched mode). This operation mode enables simultaneously a high mass resolution ($\text{FWHM } m/\Delta m > 6000$ at m/z 126.90 (I^-)) and high signal intensities. The primary ion current was about 0.6–0.65 pA and the cycle time was set to 70 μs . An analysis area of $(50 \times 50) \mu\text{m}^2$ was chosen inside the $(250 \times 250) \mu\text{m}^2$ crater (created with 40 frames per sputter step) and rasterized with 128×128 pixels at 1 shot per pixel and frame. The data analysis of the ToF-SIMS measurements was carried out with the Surface Lab Software version 7.2 (IONTOF GmbH, Muenster, Germany).

After the depth profiling, the sputter crater depths of the Scenario 3 samples were determined with a PLu neox 3D (Sensofar, Terrassa, Spain) confocal microscope. The obtained depth values were used to calibrate the sputter time axis and to determine the erosion rates for the different metals.

Results

Analysis of elemental metals

Figure 4 shows photographs of the elemental metal samples in the untreated state and after iodine treatment according to scenario 4, the roughest scenario, corresponding to 10 years of exposure in an iodine atmosphere of 0.1 Pa in space. The optical appearance of the elements Al, Fe, Ni, and Ti changed significantly during iodine treatment, suggesting that chemical reactions with iodine take place at their surfaces during treatment. The elements Cr, Mo, Ta, Nb, and W seem to have reacted much less with iodine, since their optical appearance did not change notably.

Further clarification of the chemical effect of the presence of iodine in the atmosphere surrounding the metal samples is obtained by comparing the XPS data of a corresponding untreated sample and one treated according to scenario 4 representing an upper boundary for 10 years in space in an iodine atmosphere of 1e-1 Pa. We do not expect iodine to react with the elements bonded to oxygen, since oxygen is a stronger oxidizing agent than iodine. Therefore, the focus during spectra comparison lies on the behavior of the elemental signal. Fig. 5 shows three examples of samples which exhibit strong changes of the optical appearance on iodine treatment, i.e., Ti, Al, and Fe.

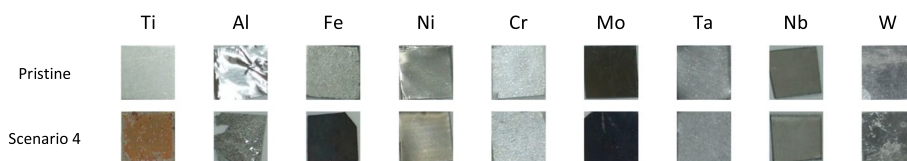


Fig. 4 Photographs of the different elemental metals in the untreated state and after treating according to scenario 4

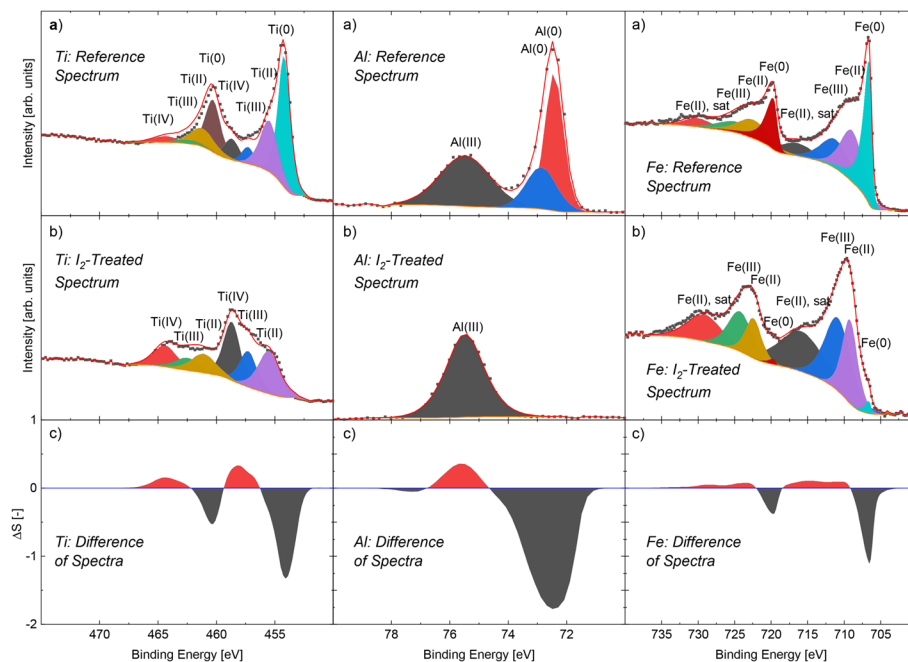


Fig. 5 XPS spectra of Ti (left), Al (center), and Fe (right) recorded from (a) an untreated reference sample and (b) an iodine-treated sample according to scenario 4. (c) shows the difference spectra according to Eq. (8). The XPS spectra of Ti, Al, and Fe were recorded in narrow-ranges about the Ti 2p, Al 2p, and Fe 2p core level signals, respectively, after 240 s of Ar⁺ etching

The Ti sample showed the most severe changes of surface appearance after iodine treatment (see Fig. 4). The XPS spectra of the treated and untreated Ti sample were recorded in the vicinity of the Ti 2p core level signals which are sensitive to the bonding environment and analyzed according to Ref. [27]. The XPS spectrum of the untreated Ti shows four spin doublets in the Ti 2p range. The turquoise peak (Ti(0)) with a binding energy (BE) of about 454 eV and the brown peak (Ti(0)) shifted by 6.1 eV to higher BE values form the doublet 2p_{3/2} and 2p_{1/2} of metallic Ti. The black/red peak doublet (459 eV and 464 eV) is assigned to Ti(IV) oxide, i.e. TiO₂. The other two 2p doublets are indicative for other titanium oxides Ti(II), i.e. TiO (2p_{3/2} at 456 eV, 2p_{1/2} at 461 eV) and Ti(III), i.e. Ti₂O₃ (2p_{3/2} at 457 eV, 2p_{1/2} at 463 eV). On the surface without Ar⁺ sputtering (spectrum not shown), the dominating oxide species is TiO₂ as expected for titanium stored in ambient atmosphere. The cleaning procedure (in an ultrasonic bath) used does not affect the oxide. A distinct signal of Ti(0) was also detected. The presence of different titanium oxides in the reference XPS spectrum shown is not surprising because the Ar⁺ sputtering (here 240 s) causes preferential etching in case of TiO₂, i.e., the oxygen content is reduced in the ion etching process.

After treating the sample with iodine, the XPS spectrum has changed significantly. The spin doublet of the metallic Ti (Ti(0)) is no longer visible and the relative signal strengths of the other spin doublets is altered. The relative strength of signals of spin doublets of Ti with higher oxide numbers has increased. The disappearance of the metallic Ti(0) signals and an increase, especially, of the Ti(IV) signals are explained by the reaction of the sample with iodine as there is no additional oxygen in the reaction vessel present which may react with the sample. Thus, the alteration of the signals originate from to the

formation of titanium iodides. For example, the increase of the Ti(IV) signal is explained by the formation of titanium(IV) iodide (TiI_4). TiI_4 is a red-brown solid, which agrees with the observation of the change of the optical appearance of the treated sample compared to the reference sample. The XPS trends can be seen even more clearly in the difference spectrum. The metallic signals strongly decrease (black curve), while the signals at positions where titanium iodides are expected experience a significant increase in signal strength (red curve). Thus, the XPS spectra reveal the strong reactivity of titanium with iodine despite the supposedly protective oxide layer. This is probably a sign that the native oxide has not formed a closed film.

Both elemental samples, that of aluminum and that of iron, also show distinct color changes after iodine treatment (see Fig. 4). The XPS spectra for Al and Fe were recorded in the regions of the corresponding 2p major core level signals. The Fe spectra are evaluated according to Ref. [28] Since Fe has a very complex peak structure with multiple peak doublets for the species of Fe(0), Fe(I), Fe(II), Fe(III) and additional satellites (with partly overlapping BE values), we use a simplified model by fitting only one peak for Fe(0), Fe(I), and Fe(III). We also are considering only one satellite labeled as “Fe(II), sat”. The fit of “Fe(II), sat” might include a satellite structure of Fe(III) which was not fitted separately. The Al spectra were analyzed following Refs [29, 30].

The XPS spectra of both reference samples again show signals characteristic for the corresponding native oxides in addition to the typical spin doublets of the metallic phase (i.e., $2p_{3/2}$ at 72 eV and $2p_{1/2}$ at 73 eV for Al(0); $2p_{3/2}$ at 707 eV and $2p_{1/2}$ at 720 eV for Fe(0)). In case of the untreated Al samples, the typical broad signature Al_2O_3 (Al(III)) is observed at 75.5 eV, whereas the untreated Fe sample shows spin doublets of FeO, i.e., Fe(II) ($2p_{3/2}$ at 709 eV and $2p_{1/2}$ at 722 eV) and Fe_2O_3 , i.e., Fe(III) ($2p_{3/2}$ at 711 eV and $2p_{1/2}$ at 725 eV). After the iodine treatment, the spin doublets of the metallic phases are drastically reduced or even disappear in the corresponding XPS spectra, while the detected signal of the spin doublets corresponding to higher oxidation states of the elements increase. Similar to Ti, Al and Fe can form iodides with high oxidation numbers of the metal ions, e.g., FeI_3 (Fe(III), black solid), FeI_2 (Fe(II), grey solid) and AlI_3 (Al(III), white solid). Thus, the signals of the metal oxides and metal iodides of the same metal oxidation state overlap. Consequently, the disappearance of the metallic signals in the XPS spectra of the iodine-treated samples and the increase of the XPS signals corresponding to the metal elements with higher oxidation states confirm the reactivity of Fe and Al with iodine despite an oxide layer. The findings are in accordance with change of the optical appearance of the iodine treated Al and Fe sample compared to the reference samples shown in Fig. 4.

Weighing the samples of the three elemental specimens of Al, Fe, and Ti, discussed above, before and after the treatment showed a detectable change of weight. The titanium sample (416.0 mg) lost 0.9% of its weight in form of red-brown material crumbs, i.e., TiI_4 , after a treatment according to scenario 4. The treatment according to the scenarios 1 to 3 did not result in a detectable weight change of the corresponding Ti sample. The Fe samples (646.2 mg in scenario 3 and 721.1 mg in scenario 4) gained about 0.14% of weight after the exposure to iodine according to scenario 3 and 0.35% after treatment as stated for scenario 4. This suggests a strong reaction of the sample with iodine, forming an increasing surface layer of iron iodides. The light weight and much thinner Al

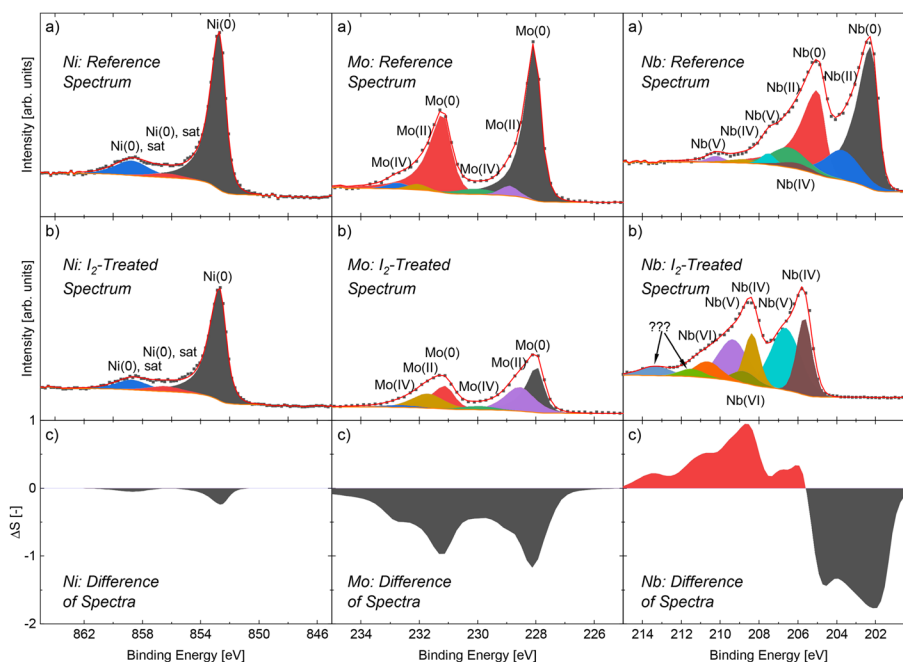


Fig. 6 XPS spectra of Ni (left), Mo (center), and Nb (right) recorded from (a) an untreated reference sample, (b) an iodine-treated sample according to scenario 4. (c) shows the difference of spectra according to Eq. 8. The XPS spectra of Ni, Mo, and Nb were recorded in narrow-ranges about the Ni 2p, Mo 3d, and Nb 3d core level signals, respectively, after 240 s of Ar⁺ etching

sample (7.9 mg in scenario 3 and 4) with a thickness of 20 μm compared to the 2 and 1 mm of the Ti and Fe samples, respectively, experienced a weight gain of 10% and 95% after treatment according to scenario 3 and 4, respectively. However, the high surface-to-volume ratio of the Al foil in conjunction with the small atomic mass of Al explains the very high relative weight gain when the aluminum iodides such as AlI₃ surface layers are formed. XPS results, optical inspection as well as the weighing results agree well and corroborate that all three metals Al, Ti, and Fe strongly react with iodine.

The narrow-range spectra of the major core level signals Cr 2p, Ta 4f, W 4f (shown in Fig. 6) were evaluated based on the Refs [28] for Cr [31, 32], for Ta, and [31] for W. Reference and treated sample of all the three metals exhibit a similar behavior. In all three cases, the surface spectrum prior to Ar⁺ etching shows a weak metallic signal along with signals of corresponding metal oxides. The signals of the compound with the metal in the highest oxidation state (i.e. Cr(III) hydroxide (Cr(III) 2p_{3/2}: 577.2 eV), Ta₂O₅ (Ta(V) 4f_{5/2}: 26.4 eV), and WO₃ (W(VI) 4f_{7/2}: 35.8 eV)), dominate the XPS spectrum. After Ar⁺ etching, the oxide compounds at the surface are removed and the asymmetric metallic peaks dominate the spectra, i.e. Cr(0) at 574.2 eV, Ta(0) at 21.2 eV, and W(0) at 30.9 eV. The iodine treatment has no effect on the XPS spectra. Oxide compounds are detectable prior to Ar⁺ etching. However, after Ar⁺ etching the metal signals of oxidation number 0 dominate. The iodine content (in molecular form) on the samples after etching was 14 at.% (Cr-sample), 5 at.% (Ta-sample), and 7 at.% (W-sample) at the surface. The difference spectra of all three samples underline again that iodine treatment has almost no effect on these specimens.

The surface of the Ni sample after iodine treatment shows a change of optical appearance compared with the surface of the reference sample (see Fig. 4) which suggests that the sample has reacted with iodine. However, a close analysis of the XPS spectra taken in the Ni 2p region (Fig. 6), revealed no difference between the reference and treated sample. The XPS spectra of the reference and the treated sample were fitted based on parameters given by Biesinger [33]. In both spectra, the Ni 2p_{3/2} region shows only the main metallic signals (Ni(0) at about 853 eV). None of the detected peaks arise from Ni in a higher oxidation state, e.g. Ni(II) of NiI₂ [34]. However, a distinct iodine signal was detected in the I 3d region at 619.6 eV (not shown) indicative for molecular iodine. Even after 240 s of Ar⁺ etching, the iodine made up about 24 at.% of the detected elements. The surface spectra (prior to Ar⁺ etching) showed typical oxide and metallic peak structures of Ni. Therefore, Ni seems to be resistant against the iodine treatment and did not form iodide compounds. The change in optical appearance of the Ni is therefore attributed to a deposition of molecular iodine on the surface.

The model for fitting the Mo 3d XPS region is based on the publication by Alov [31]. The character of the changes of the XPS spectra is similar to those of the metals Cr, Ta, and W in the sense, that the XPS spectra recorded at the surface prior to Ar⁺ etching show strong oxide-related peaks in the same spectral region as those of metallic species.

Prior to Ar⁺ etching, the XPS spectra (not shown in the figure) recorded on the surfaces of the reference and the iodine-treated sample exhibit a signal corresponding to Mo(IV) in MoO₃, which dominates over a small metallic peak Mo(0). After 240 s of Ar⁺ etching, as can be seen in Fig. 6, the metallic peaks (Mo(0) 3d_{5/2}: 228.0 eV) dominate and multiple oxide peaks with lower oxidation number (Mo(II), Mo(IV)) occur in the spectra of both, the reference and the iodine-treated sample. The intensity ratio of the Mo(0) signal and the Mo(II) signal in the iodine-treated sample is somewhat smaller than in the reference sample, but the Mo(0) signal is still dominant. The corresponding difference spectrum shows a distinct negative area which reflects the significant difference in signal strength between the iodine-treated and the reference XPS spectrum. The detected Mo 3d signals from the treated Mo sample are much lower, about 20% of the corresponding reference signals. The amount of molecular iodine detectable in the sample region studied by XPS was about 26 at.% after iodine treatment. The presence of iodine damps the Mo XPS signals obtained in case of the treated sample, which is not compensated by the calculation procedure of the difference spectrum (ΔS). Since the difference spectrum does not show a positive area nor a peak movement, the overall differences of the reference and iodine treated spectrum is small and let us conclude that Mo, if at all, only weakly chemically reacts with iodine.

The XPS spectra of Nb 3d region were interpreted following the peak assignments Yang et al. [35] and Geyer-Lippmann et al. [36]. The recorded surface XPS spectra of the iodine-treated and the reference sample (not shown) are almost identical. In both cases, the peak structure is similar to the XPS spectrum reported by Yang et al. [35] for Nb-samples exposed to molecular oxygen (air). The dominant peak doublet of Nb(V) (Nb(V) 3d_{5/2}: 207.1 eV) is assigned to Nb₂O₅, while the less pronounced peak doublets are representing NbO₂ (Nb(IV)) and NbO (Nb(II)) compounds as well as metallic Nb (Nb(0) 3d_{5/2}: 201.7 eV). After 240 s of Ar⁺ etching, the peak structure of the reference sample shifts towards lower BE values. The dominant XPS signal is now the metallic

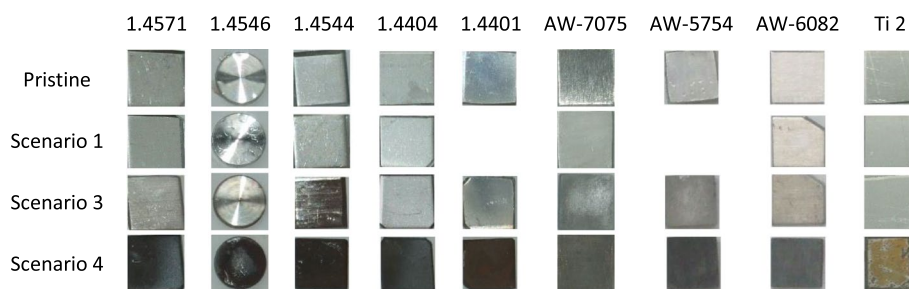


Fig. 7 Alloy samples (1.XXXX – stainless steel alloys, AW-XXXX – aluminum alloys) after an iodine treatment according to the different scenarios

Nb(0) doublet. However, weaker signals of Nb(II), Nb(IV), and Nb(V) can also be seen in Fig. 6. In contrast, the XPS spectrum of the iodine-treated Nb sample after 240 s of Ar^+ etching is dominated by the double peak structure of Nb(V) and the Nb(0) doublet has vanished. Furthermore, multiple additional peak doublets appear either side of the Nb(V) doublet peaks. In particular, the relative increase in signal strength of the Nb(IV) doublet peaks compared to the other signals suggests that NbI_4 is formed in addition to the residual NbO_2 also present in the reference sample. The signals marked by question marks at higher BE values of about 212 eV and 214 eV are tentatively assigned to Nb in oxidation states larger than +5, which is somewhat uncommon for metallic samples after etching. Nevertheless, similar observations were made by Geyer-Lippmann et al. [36] in their analysis of various niobium-iodides. Those authors have assigned the additional peaks to higher oxidized compounds and oxide iodides. Thus, Nb seems not to react with an iodine atmosphere when treated according to scenario 4, since the surface spectra of the treated and reference sample look identical, including the metallic peak. Nevertheless, the combination of Ar^+ etching and prior iodine treatment changes the surface structure in an untypical way for metallic samples. Hence, Nb is not really inert to reactions with iodine.

Analysis of alloys

In the previous section, we have shown that the main constituents of most metal alloys such as Al, Fe, and Ti strongly react with iodine, while the majority of tested minor constituents of the alloys such as the elements Cr, Ni, Mo, W, or Ta are not affected by the iodine treatment. In our experiments, all alloy samples studied (stainless steel and aluminum alloys) eventually changed their optical appearance with extended iodine exposure, as presented in Fig. 7, suggesting chemical reactions with iodine. However, none of the treated samples shows any visual change of appearance when treated with iodine according to scenario 1 and 2. Treatment in scenario 3 leads to an obvious color change of some of the samples, e.g., the stainless-steel sample 1.4544 or the aluminum alloy AW-7075. The survey XPS spectra of many of the samples show a distinct iodine signal, proving the iodine contamination of the surface. Thus, the amount of iodine must reach a certain threshold to have a distinct visual effect on a sample, since the different treatment scenarios do not change the chemical reactions between iodine and the respective elements, as explained in the first section. The color change is a strong indication that

an iodine related layer with thicknesses at least a couple of hundred nanometers forms at the surface during treatment.

To examine the thickness of the surface layer and the iodine diffusion behavior, ToF-SIMS depth profiling was applied. For these measurements, the samples Ti 2, AW-7075, and 1.4544 were selected as representative of the three materials groups, i.e., titanium, aluminum alloy, and stainless steel. Furthermore, the selected samples are those exhibiting the strongest color change in their respective material group. Therefore, we assume that they are most affected by the iodine treatment. For evaluation of iodine diffusion, the diffusion profiles of the I^- signal were used. Figure 8a) depicts the recorded depth profiles of the I^- signal of the samples of the selected material groups treated according to the scenarios 3 and 4, respectively. Near the surface, all diffusion profiles start with a flat, relatively constant iodine signal, which we assign to an iodine layer on the surface. The depth ranges where iodine signals are detected with constant intensity agree with the corresponding values of the surface roughness of the samples. This finding somewhat suggest that the depth range does not correspond to the layer thickness of the iodine surface layer, but is rather caused by the surface roughness which leads to a partial screening of the surface from the ion beam used for etching. Therefore, we believe that the surface coverage by iodine is much thinner.

Below, iodine diffusion within the bulk surface is shown. Here, the I^- signals decrease rapidly (almost exponentially) with increasing depths until constant background signal intensities of I^- are reached. In depth ranges prior to approaching the background signal, the iodine signal decreases more slowly with depth (i.e., the slope in the logarithmic plot, not shown, becomes flatter). These signals are probably due to iodine atoms diffusing along grain boundaries, since the activation energy of this migration process is lower than that for lattice diffusion in the bulk of the grains [37].

The iodine signal detected for the stainless-steel sample 1.4544 (treatment scenario 4) shows a different diffusion behavior. Throughout the complete depth profile of about

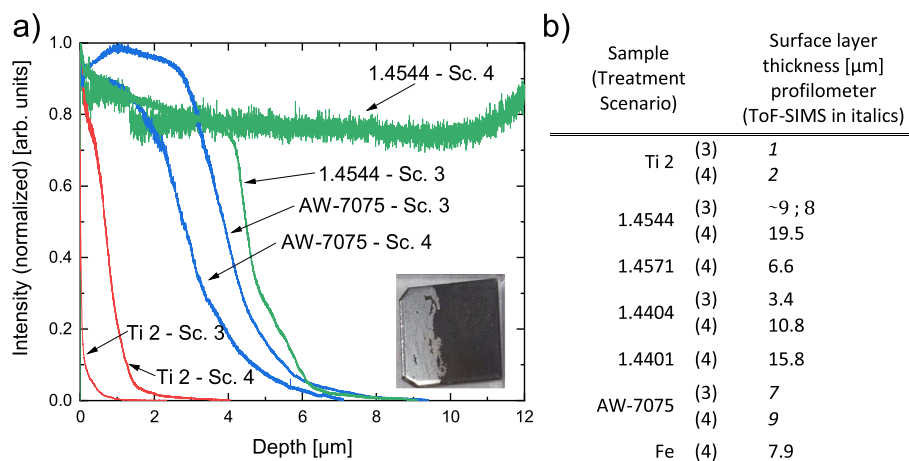


Fig. 8 **a** ToF-SIMS surface depth profiles show the iodine diffusion behavior of the iodine-contaminated samples Ti 2 (red), AW-7075 (blue), and 1.4544 (green), treated according to scenarios 3 and 4. The inset shows the sample 1.4404 as prepared for the profilometer measurements. **b** Thickness of the discolored surface layers using ToF-SIMS and profilometer measurements of samples treated according to scenarios 3 and 4

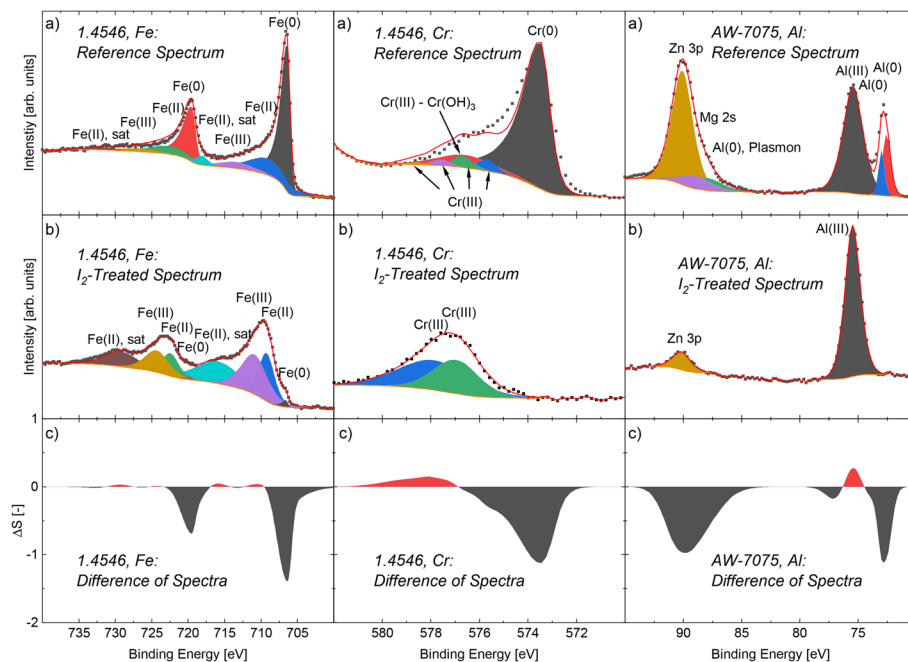


Fig. 9 Fe 2p and Cr 2p XPS spectra (left and center) recorded from (a) an untreated and (b) an iodine-treated piece of stainless steel 1.4546 sample. Al 2p XPS spectra (right) recorded from (a) an untreated and (b) an iodine-treated Al-based metal alloy EN AW-7075 sample. The iodine treatment corresponds to 10 y in 1e-1 Pa iodine partial pressure (scenario 4). The corresponding difference spectra (c) are shown below

12.4 μm , the signal intensity of iodine does not decrease, suggesting that iodine could diffuse deeper than 12 μm into the sample. Therefore, in a subsequent measurement, we removed the chemically reacted, black surface layer with a paper towel on parts of the sample's surface until the shiny metallic surface reappeared. The detected height difference between the dark treated surface and the shiny cleaned surface area is about 19.5 μm (see Fig. 8b)) and marks the maximal depth of the eroded surface layer. We believe that the chemical reaction between iodine and iron oxide at the surface destroyed the surface morphology, since a reaction between these two reactants is accompanied by a significant volume change that cracks grain boundaries and enables additional iodine to diffuse to larger depths [12].

The iodine diffusion depth for all samples analyzed is in the range of a few tens of μm only, which is, in comparison to a total sample thickness of 1–3 mm, not significant. Corrosion of the metals and metal alloys by iodine can be considered a surface effect and does not affect the integrity of the bulk of the material. Therefore, it can be assumed that the stability of macroscopic structural elements of the satellite made of such metals or metal alloys will be given for the entire duration of the mission.

For a detailed analysis of the chemical reactions, the stainless steel samples 1.4546 and 1.4544 were closely analyzed using XPS prior and after iodine treatment according to scenario 4. An untreated sample served as reference sample. We attempted to record narrow-range spectra of the major core level signals of all elemental constituents of the stainless steel alloy. Unfortunately, only signals of the elements present in larger quantities, i.e., Fe, Cr, and Ni were detectable. An adequate Ni 2p signal was only measured for the reference samples and will not be further discussed. The recorded XPS spectra

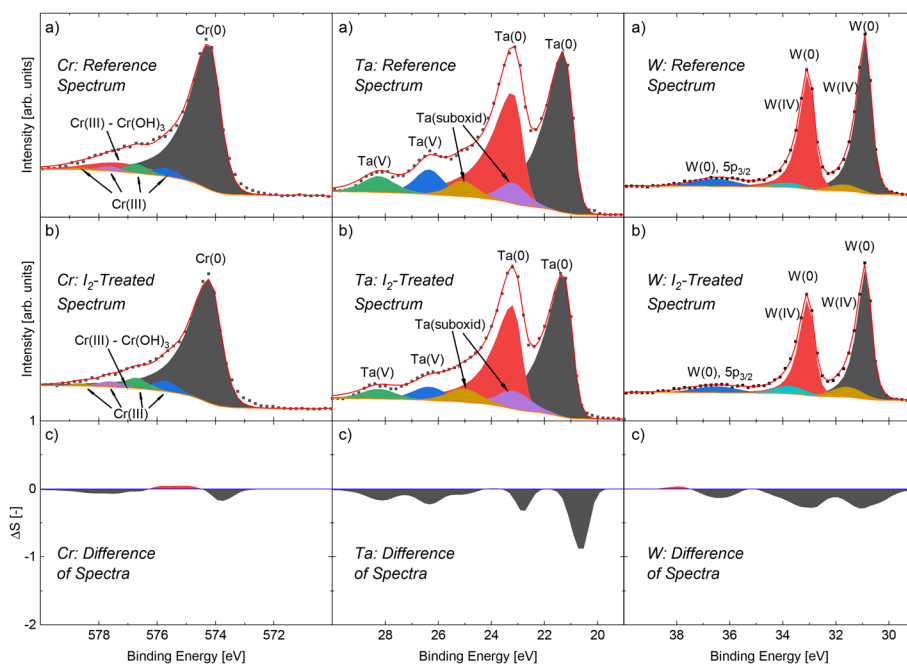


Fig. 10 XPS spectra of Cr (left), Ta (center), and W (right) recorded from (a) an untreated reference sample and (b) an iodine-treated sample according to scenario 4. (c) shows the difference of spectra according to Eq. (8). The XPS spectra of Cr, Ta, and W were recorded in narrow-ranges about the Cr 2p, Ta 4f, and W 4f core level signals, respectively, after 240 s of Ar⁺ etching

from the sample 1.4546 are shown in Fig. 9 for the Fe 2p and the Cr 2p region (note, the XPS spectra of the stainless steel 1.4544 show the same trends and are not discussed further). As expected based from the analysis of the elemental metals, the Fe 2p signal of the reference sample shows three spin-doublets and a pair of satellites after 240 s of Ar⁺ etching. The strongest doublet (purple and yellow) originates from Fe(0) of metallic iron, while the other signals originate from higher oxidation states of iron, i.e., Fe(II) and Fe(III). In the XPS spectrum of the corresponding iodine-treated sample, the Fe(0) doublet has virtually disappeared and the Fe(II) and Fe(III) doublets dominate indicating that Fe has reacted with iodine forming, e.g., FeI₂ or FeI₃, as discussed in the [elemental metals](#) section. The corresponding Cr 2p XPS spectrum recorded from the untreated sample 1.4546 agrees with that recorded from the untreated elemental Cr-sample (see Fig. 10), including a spin-doublet representing pure chromium. In contrast, the analysis of the Cr2p core-level XPS spectrum of the iodine-treated stainless steel sample 1.4546 differs from that of the iodine-treated elemental Cr sample in Fig. 10. The iodine-treated stainless steel sample exhibits no Cr(0) signal in its XPS spectrum, but only two spin doublets at higher BE values both assigned to Cr(III) 2p_{3/2}. Thus, it seems that Cr atoms in the alloy react and form bonds with iodine other than in the elemental Cr metal. This finding suggests that the chemical reaction of an element with iodine is not only to depend on the element itself, but also on the nearest-neighbor atomic environment. On the one hand, this makes it difficult to judge the iodine-resistance of an alloy solely by the properties of its elemental constituents. On the other hand, there is also a certain probability that in alloys exist which are inert to iodine.

Samples of the Al-based alloy EN AW-7075 were also analyzed by XPS. The narrow range Al 2p spectra of the reference and iodine-treated sample after 240 s of Ar⁺ etching are shown on the right of Fig. 9. The Al 2p signals in the XPS spectra of both samples behave similarly to the signals recorded on comparable elemental Al samples presented in Fig. 5. The peaks representing aluminum in the metallic state Al(0) disappear after iodide treatment and only one Al 2p peak remains, which represents aluminum oxide or iodide. In contrast to the elemental spectrum after iodine treatment, a significant peak at the high BE side confirms the presence of the alloy elements Mg and Zn. The detected peak comprises contributions from signals of Zn 3p, Mg 2s, and an Al-plasmon (also shown in the Al elemental spectrum). It is worth noting, that the intensity of the elemental constituents Mg and Zn drastically decreases with increasing duration of the iodine treatment, suggesting that they are removed by an erosion process. The aluminum alloy chemically reacts with the iodine as it was expected based on the analysis of the elemental Al sample. The comparatively high mass fractions of the minor elemental constituents do not provide protection of the aluminum. On the contrary, the results show that iodine severely erodes aluminum alloys. Therefore, stainless steel alloys should be favored over aluminum alloys when a usage in iodine-environments is anticipated.

Conclusions

Using iodine as propellant for electric propulsion systems has many advantages. The chemical reactivity of iodine is commonly considered as the major disadvantage. Hence, materials for structural parts of a satellite have to be carefully selected or protected. We define and justify a measurement protocol enabling us to mimic the conditions experienced by satellite components in typical mission scenarios of satellites propelled with iodine-fed electric thrusters and to extract an upper limit for the damage caused during a 10-year mission. In such dry, non-humid environments with low-iodine partial pressures below 1e-1 Pa and anticipated mission durations of 10 years, the elemental metals such as Cr, Mo, Ni, Ta, and W are resistant against iodine in its elemental form. However, Nb, Al, Ti, and Fe similar to Cu [13, 16] strongly react with iodine under these conditions. Our results confirm the findings of Beck et al. [38] that the reactivity towards iodine decreases from Fe via Ni to Cr. In case of Al and Ti treated by these conditions, the chemical reaction products even cause brittleness of the surface and deterioration of the structural integrity of the material in the vicinity of the surface. Nevertheless, the corrosion can be considered a surface effect despite the long duration of the mission. The maximum depth of the corroded layer in the samples studied was about 20 μm for stainless steel treated according to the harshest scenario 4. We also studied metal alloys, in particular, various stainless steels and aluminum alloys. The main elemental constituents of the two types of alloys, Fe and Al, both react with iodine. In case of the Al alloy studied, the elements acting as minor constituents of the alloy are Zn, Mg, and Cu which all three can react strongly with iodine [17, 39]. Thus, it is not surprising that the aluminum alloy basically behaves like the elemental Al metal under iodine treatment. Alloying with minor fractions of iodine-resistant elements such as Cr, Mo, Ni, Ta, or W, as it is done in case of stainless steels 1.4546 (with Cr, Ni, Nb) and 1.4546 (with Cr, Ni, Ti), cannot remedy the effect of iodine on the main stainless steel constituent Fe. It even turns out that Cr in stainless steel reacts with iodine, although it is resistant to iodine in Cr metal.

This reflects the basic knowledge that the reactivity of chemical element at given conditions not only depends on the reaction partner (here iodine), but also on the element's atomic nearest-neighbor environment. In other words, surrounding a Cr atom by other Cr atoms as in the corresponding metal constitutes a stable environment suppressing the reaction with iodine. A change of atomic environment of a chemical element may either strengthen or weaken its resistance to reacting with iodine. Following this line of reasoning implies that it cannot be ruled out that an iodine resistant material may be obtained by atomic alloying, however, such alloy compositions have not been identified yet. An option may be high-grade alloy steels with high fractions of the resistive constituents Cr, Mo, Ni, Ta, and W such that the Fe nearest-neighbor environment is significantly altered compared to Fe metal. A possible candidate for such an alloy is stainless steel 1.4536 (X1NiCrMoCu25–20–5), which should be investigated. Another rather self-evident option of improving the resistance of a metal or metal alloy to iodine is applying a protective surface coating with an iodine-resistant metal such as Cr, Mo, Ni, Ta, or W or a closed oxide film. It is of paramount importance that such a protective surface coating is dense and closed. In particular, our experiments show that the native oxides, for example, in case of Al are not sufficient to suppress a reaction between iodine and Al. As oxygen is a stronger oxidizing agent than iodine, this shows that the native Al_2O_3 layer is not dense enough to provide a suitable protection layer as it can be overcome by iodine. However, we have shown that the deteriorating effect of iodine is basically non-existent even for highly reactive materials such as Ti or Al at low iodine partial pressure below $1\text{e-}3$ Pa at an anticipated exposure time of 10 years (scenario 1 and 2). Since higher partial pressures of iodine are only expected inside the propellant feed system and the thruster, the principal satellite structures and components should not be affected by the surrounding iodine atmosphere and do not need adaptation.

In conclusion, all elemental metals and metal alloys studied are only affected by iodine in a thin surface layer anticipating a space environment with an iodine partial pressure of $1\text{e-}1$ Pa and a mission duration of 10 years. The structure of the bulk of the metals studied is not affected, only the optical appearance is altered. This implies that macroscopic structural elements of the satellite made of those metals should preserve their stability for the entire duration of the mission. Furthermore, several metals are in these dry reaction conditions basically inert to iodine even over the long time span of a typical space mission duration. The possibilities of identifying additional iodine resistant alloys and of applying protective coatings of iodine-resistant metals or other materials offers various ways of overcoming the challenge of iodine reactivity on components exposed to a dense iodine atmosphere on satellites or other spacecraft equipped with iodine-fed thrusters.

Acknowledgments

This project has received funding from the European Union's Horizon 2020 research and innovation program under grant agreement No. 870336 (Project iFACT). Daniel Zschätzsch is grateful for a PhD grant in the framework of the graduate school "Radio-frequency ion thrusters" of Justus Liebig University and Ariane Group. We also acknowledge funding by the European Community for ERDF Innovation Laboratories "High-Performance Materials" and "Rough Ambient Physics" and the Deutsche Forschungsgemeinschaft (DFG) via the RTG (Research Training Group) 2204 "Substitute Materials for sustainable Energy Technologies".

Code availability

Not applicable.

Authors' contributions

Max Vaupel and Franz G. Hey selected the materials and provided the majority of samples. Material treatment, data analysis, and creation of the first draft of the manuscript was performed by Daniel Zschätzsch. Sebastian L. Benz conducted

the XPS measurements and decisively supported the analysis of the XPS data. Peter J. Klar supervised the work. Jürgen Janek helped to develop the thermo-chemistry model for the iodine reactions. Kristof Holste supervised the laboratory work. Christine Kern conducted and evaluated the ToF-SIMS measurements to determine the depth of iodine diffusion into the samples' surfaces. All authors contributed to the study conception and design and commented on previous versions of the manuscript, read and approved the final manuscript.

Funding

Open Access funding enabled and organized by Projekt DEAL. This project has received funding from the European Union's Horizon 2020 research and innovation program under grant agreement No. 870336 (Project iFACT). Daniel Zschätzsch is grateful for a PhD grant in the framework of the graduate school "Radio-frequency ion thrusters" of Justus Liebig University and Ariane Group. We also acknowledge funding by the European Community for ERDF Innovations Laboratories "High-Performance Materials" and "Rough Ambient Physics" and the Deutsche Forschungsgemeinschaft (DFG) via the RTG (Research Training Group) 2204 "Substitute Materials for sustainable Energy Technologies". We would like to thank Mathias Wickleder (U. Cologne) for fruitful discussions.

Availability of data and materials

The datasets generated and analyzed during the current study are available in a database: <https://doi.org/10.22029/jlupub-441> [22]. Additional data is available upon reasonable request to the authors.

Declarations

Competing interests

The authors have no competing interests to declare that are relevant to the content of this article.

Received: 17 May 2022 Accepted: 18 September 2022

Published online: 28 September 2022

References

1. Holste K et al (2020) Ion thrusters for electric propulsion: scientific issues developing a niche technology into a game changer. *Rev Sci Instrum* 91:061101. <https://doi.org/10.1063/5.0010134>
2. O'Reilly D, Herdrich G, Kavanagh DF (2021) Electric propulsion methods for small satellites: a review. *Aerospace* 8:22. <https://doi.org/10.3390/aerospace8010022>
3. Lev D et al (2019) The technological and commercial expansion of electric propulsion. *Acta Astronaut* 159:213–227. <https://doi.org/10.1016/j.actaastro.2019.03.058>
4. Betancourt, M. L. R., Bögela, E., Collier-Wright, M., Wilcox, J. L. & Kaplan, P. A. Comparative Overview of Nuclear Electric Propulsion Programs and Concepts (2021). IAC-21,C3,5-C4.10,2,x64835
5. Rafalskyi D et al (2021) In-orbit demonstration of an iodine electric propulsion system. *Nature* 599:411–415. <https://doi.org/10.1038/s41586-021-04015-y>
6. Manente, M. et al. REGULUS: iodine fed plasma propulsion system for small satellites. (2019)
7. Sidky PS (1998) Iodine stress corrosion cracking of Zircaloy reactor cladding: iodine chemistry (a review). *J Nucl Mater* 256:1–17. [https://doi.org/10.1016/S0022-3115\(98\)00044-0](https://doi.org/10.1016/S0022-3115(98)00044-0)
8. Fukuda T, Omori S (1974) Corrosion of AISI 316 and AISI 304 stainless steel with iodine vapor. [https://doi.org/10.2172/7039340http://www.osti.gov/servlets/purl/7039340/](https://doi.org/10.2172/7039340http://www.osti.gov/servlets/purl/7039340)
9. Beavers JA, Berry WE, Griess JC Materials performance in off-gas systems containing iodine (ORNL/Sub-7327/11, 6040920), 7327–116040920. <https://doi.org/10.2172/6040920>
10. Amend J, Dillmann H-G, Furrer J, Kaempffer R (1985) 1000 h-Langzeituntersuchungen zur Iod-Korrosion an ausgewählten Edelstahlproben unter simulierten Auflöserbedingungen. Kernforschungszentrum Karlsruhe. <https://core.ac.uk/download/pdf/197571432.pdf>
11. Funke F, Greger G-U, Hellmann S, Bleier A, Morell W (1996) Iodine-steel reactions under severe accident conditions in light-water reactors. *Nucl Eng Des* 166:357–365. [https://doi.org/10.1016/S0029-5493\(96\)01253-8](https://doi.org/10.1016/S0029-5493(96)01253-8)
12. Wren JC, Glowa GA, Merritt J (1999) Corrosion of stainless steel by gaseous I₂. *J Nucl Mater* 265:161–177
13. Branam R (2016) Iodine plasma (electric propulsion) Interaction with Spacecraft Materials
14. Costa G, Benavides GF, Kulis MJ, Setlock J (2020) Corrosion Behavior of Stainless Steel 304 and Nickel 625 Under Iodine Vapor at 300 °C 21
15. Szabo J et al (2013) Iodine propellant space propulsion. IEPIC https://www.researchgate.net/publication/305700508_Iodine_Propellant_Space_Propulsion
16. Martínez JM, Rafalskyi D (2021) Design and development of iodine flow control systems for miniaturized propulsion systems. *CEAS Space J*. <https://doi.org/10.1007/s12567-021-00384-2>
17. Benavides GF, Kamhawi H, Mackey JA, Haag TW, Costa GCC (2018) Iodine hall-effect electric propulsion system research. *Dev Syst Durabil Demon* 32. <https://doi.org/10.2514/6.2018-4422>
18. Ley W, Wittmann K, Hallmann W (2019) Handbuch der Raumfahrttechnik. Hanser 978-3-446-45429-3
19. Levko D, Raja LL (2021) Fluid modeling of inductively coupled iodine plasma for electric propulsion conditions. *J Appl Phys* 130:173302. <https://doi.org/10.1063/5.0063578>
20. Dietz P et al (2019) Molecular propellants for ion thrusters. *Plasma Sources Sci Technol* 28:084001. <https://doi.org/10.1088/1361-6595/ab2c6c>
21. Dietz P, Becker F, Keil K, Holste K, Klar PJ (2020) Performance of a rf neutralizer operating with noble gases and iodine. *Eur Phys J Appl Phys* 91:10901. <https://doi.org/10.1051/epjap/2020190213>
22. Zschätzsch D, Klar PJ (2021) Iodine Materials Interaction Database. <https://doi.org/10.22029/jlupub-441>

23. Atkins PW, De Paula J (2006) *Atkins' Physical chemistry*. W.H. Freeman OCLC: 66528976a. ISBN: 978-0-7167-8759-4
24. Kubaschewski O, Alcock CB, Spencer PJ, Kubaschewski O (1993) *Materials thermochemistry*. Pergamon Press ISBN: 978-0-08-041889-6 978-0-08-041888-9. <https://www.amazon.com/dp/0080418880/ref=olp-opf-redir?ad=1&condition=used&tag=bookfinder-test-b2-20>
25. (1998) NIST-JANAF thermochemical tables. American Chemical Society; American Institute of Physics for the National Institute of Standards and Technology. 978-1-56396-820-4
26. Washington RA, Naldrett SN (1955) Preparation of pure, Dry Iodine. *J Am Chem Soc* 77:4232. <https://doi.org/10.1021/ja01621a020>
27. Biesinger MC, Lau LWM, Gerson AR, Smart RS (2010) Resolving surface chemical states in XPS analysis of first row transition metals, oxides and hydroxides: Sc, Ti, V, Cu and Zn. *Appl Surf Sci* 257:887–898. <https://doi.org/10.1016/j.apsusc.2010.07.086>
28. Biesinger MC et al (2011) Resolving surface chemical states in XPS analysis of first row transition metals, oxides and hydroxides: Cr, Mn, Fe, Co and Ni. *Appl Surf Sci* 257:2717–2730. <https://doi.org/10.1016/j.apsusc.2010.10.051>
29. Rotole JA, Sherwood PMA (1998) Aluminum foil by XPS. *Surf Sci Spectr* 5:4–10. <https://doi.org/10.1116/1.1247850>
30. Kumar N, Biswas K (2019) Cryomilling: an environment friendly approach of preparation large quantity ultra refined pure aluminium nanoparticles. *J Mater Res Techn* 8:63–74. <https://doi.org/10.1016/j.jmrt.2017.05.017>
31. Alov NV (2005) Determination of the states of oxidation of metals in thin oxide films by X-ray photoelectron spectroscopy. *J Anal Chem* 60:431–435. <https://doi.org/10.1007/s10809-005-0114-x>
32. Zier M, Oswald S, Reiche R, Wetzig K (2003) XPS investigations of thin tantalum films on a silicon surface. *Anal Bioanal Chem* 375:902–905. <https://doi.org/10.1007/s00216-003-1788-2>
33. Biesinger MC, Payne BP, Lau LWM, Gerson A, Smart RS, C. (2009) X-ray photoelectron spectroscopic chemical state quantification of mixed nickel metal, oxide and hydroxide systems. *Surf Interface Anal* 41:324–332. <https://doi.org/10.1002/sia.3026>
34. Biesinger MC, Lau LWM, Gerson AR, Smart RS (2012) C. the role of the auger parameter in XPS studies of nickel metal, halides and oxides. *Phys Chem Chem Phys* 14:2434–2442. <https://doi.org/10.1039/c2cp22419d>
35. Yang Z et al (2018) XPS studies of nitrogen doping niobium used for accelerator applications. *Appl Surf Sci* 439:1119–1126. <https://doi.org/10.1016/j.apsusc.2017.12.214>
36. Geyer-Lippmann J, Simon A, Stollmaier F (1984) Photoelektronenspektroskopie an Niobdioxiden. *Z Anorg Allg Chem* 516:55–66. <https://doi.org/10.1002/zaac.19845160909>
37. Shewmon, P. G. *Diffusion in solids*. Minerals, Metals & Materials Society, 1989. 978-3-319-48564-5
38. Beck CL et al (2021) Molecular iodine interactions with Fe, Ni, Cr, and Stainless Steel Alloys. 8. <https://doi.org/10.1021/acs.iecr.0c04590>
39. Parsons LB (1925) The influence of water on certain chemical reactions. Iii. The reactions between certain metals and iodine. *J Am Chem Soc* 47:1830–1835. <https://doi.org/10.1021/ja01684a007>

Publisher's Note

Springer Nature remains neutral with regard to jurisdictional claims in published maps and institutional affiliations.